(Received 5 November 2025, Accepted 24 November 2025, Scheduled 18 December 2025)

Design of a Compact High-temperature Superconducting Bandpass Filter with Mixed Electromagnetic Coupling

Chenhao Xu[1], Chenchen Wang[3], Yiqiuzi Shen[1], and Liguo Zhou[1,2,*]

[1] School of Health Science and Engineering, University of Shanghai for Science and Technology, Shanghai 200093, China
[2] Terahertz Technology Innovation Research Institute, University of Shanghai for Science and Technology, Shanghai 200093, China
[3] School of Optoelectronic Information and Computer Engineering, University of Shanghai for Science and Technology Shanghai 200093, China

ABSTRACT: This paper systematically analyzes the electromagnetic coupling characteristics between microstrip resonators and proposes a novel structure that enables mutual cancellation of electromagnetic coupling, effectively reducing the spacing between resonators. Based on this approach, a 14th-order compact high-temperature superconducting (HTS) microstrip bandpass filter is designed and implemented. By constructing a folded symmetric resonator structure to minimize the total electromagnetic coupling energy, and by optimizing the non-uniform coupling gaps in conjunction with the coupling characteristics, precise control of the coupling paths is achieved, leading to a significantly enhanced compactness. The filter is fabricated using double-sided YBCO HTS thin films and tested at liquid nitrogen temperature (77 K). Both simulation and measurement results show that the filter operates within the $0.96 \sim 1.06$ GHz frequency band, exhibits an insertion loss below 0.4 dB, an out-of-band rejection better than 78 dB, and a passband edge roll-off rate exceeding 60 dB/MHz, demonstrating excellent performance in terms of low loss, wide bandwidth, and high suppression.

1. INTRODUCTION

Bandpass filters (BPFs) are critical components in microwave and radio-frequency systems, widely used in wireless communications, navigation, positioning, and radar detection. They play an essential role in signal selection and suppression of out-of-band interference [1, 2]. With the rapid advancement of wireless communication technologies and radar systems, the performance requirements for BPFs have become increasingly stringent. In particular, in high-frequency and highly integrated systems, filters are expected not only to meet basic requirements such as low insertion loss and compact size but also to exhibit excellent out-of-band rejection and steep passband roll-off, enabling them to handle various interferences and noise in complex electromagnetic environments [3–7]. As a result, optimizing the frequency selectivity and rejection capability of filters within compact size constraints has become a significant challenge in current designs.

To address the above challenges, extensive research has focused on developing innovative filter design methods from the perspectives of coupling topology and resonator configuration. One line of work concentrates on optimizing the coupling mechanisms by introducing mixed electric-magnetic coupling, source-load coupling, and other coupling schemes [8, 9]. These approaches enable fine control of the energy transfer paths and electromagnetic field distribution among the resonators, thereby significantly enhancing the passband-edge roll-off and improving stopband rejection for a given filter order. Another line of research emphasizes resonator miniaturization, for example by employing folded open-loop resonators [10] and stepped-impedance hairpin resonators [11], which effectively reduce the circuit footprint while maintaining low insertion loss and simultaneously preserving or improving frequency selectivity and out-of-band suppression. Overall, these studies have achieved notable progress in enhancing filter selectivity, strengthening out-of-band rejection, and reducing circuit size. Nevertheless, the achievable performance remains fundamentally constrained by the intrinsic losses of conventional metallic conductors.

Given the performance limitations imposed by the inherent loss of conventional metallic conductors, high-temperature superconducting (HTS) materials have emerged as a promising pathway for enhancing bandpass filters, owing to their exceptionally low loss and high-quality factors [12–16]. For instance, [17] presented a multiple-transmission zero microstrip bandpass filter based on HTS thin films, which introduced an auxiliary coupling path between the source and middle resonator to generate a pair of transmission zeros, thereby improving filter selectivity and out-of-band rejection. A miniaturized design scheme addressing issues related to structural size and parasitic responses in HTS filters, utilizing modified spiral interdigital resonators, was proposed in [18]. This approach enhanced the suppression of spurious frequencies and extended the stopband range, resulting in further overall performance improvement. Furthermore, [19] reported an HTS bandpass filter employing dual-mode resonators, which incorporated multiple internal coupling paths and controlled zero placement to improve out-of-band rejection and passband roll-off characteristics effectively. Although these existing HTS filter designs have provided valuable insights into structural design and performance

* Corresponding author: Liguo Zhou (zlg@usst.edu.cn).

optimization, there remains considerable room for further improvement, particularly in achieving low insertion loss, high out-of-band rejection, and sharp passband roll-off under compact size constraints.

This paper presents a high-order HTS bandpass filter structure based on the manipulation of mixed electromagnetic coupling, aiming to achieve high-performance filtering characteristics within a compact layout. The proposed topology integrates symmetrically-folded resonators with non-uniform coupling gaps, enabling effective control over the strength and polarity of inter-resonator electromagnetic coupling. Based on this approach, a 14-pole HTS filter prototype has been designed and fabricated. Both simulated and measured results demonstrate excellent performance in terms of passband insertion loss, out-of-band rejection, and frequency selectivity, thereby validating the effectiveness of the proposed design methodology.

2. MIXED ELECTROMAGNETIC COUPLING

Mixed electromagnetic coupling is an integrated coupling mechanism that synergistically combines electric and magnetic interactions to enable dual-channel energy transfer through a single physical path. Its underlying principle relies on structural configurations that simultaneously introduce electric and magnetic coupling channels between resonators, allowing both types of coupling to overlap and interact cooperatively in the frequency domain spatially. Electric coupling primarily arises from fringing electric fields between adjacent conductive structures, whereas magnetic coupling originates from mutual inductive effects between current-carrying loops. Fig. 1(a) illustrates a typical topology implementing mixed electromagnetic coupling, where adjacent resonators are coupled through both a magnetic path (labeled "M") at the upper section and an electric path (labeled "E") at the lower section. Fig. 1(b) shows the corresponding equivalent circuit of a second-order mixed electromagnetic coupling structure.

Under high-frequency conditions, an individual resonator can typically be modeled as a resonant structure composed of lumped capacitance C and inductance L, with its intrinsic resonant frequency given by $f_0 = 1/2\pi\sqrt{LC}$. When two structurally similar resonators are placed in close proximity, coupling arises between them. This coupling includes not only the electric interaction represented by a coupling capacitance C_m, but also magnetic coupling due to circulating currents, represented by a mutual inductance L_m. These two effects coexist, forming what is known as a mixed electromagnetic coupling mechanism. Under this mechanism, two distinct modal frequencies are excited between the resonators, corresponding to coupling modes dominated by electric or magnetic interactions, respectively. These modal frequencies are expressed as [20]:

$$f_e = \frac{1}{2\pi\sqrt{(L-L_m)(C-C_m)}} \tag{1}$$

$$f_m = \frac{1}{2\pi\sqrt{(L+L_m)(C+C_m)}} \tag{2}$$

Here, f_e corresponds to the modal frequency dominated by electric coupling, while f_m is primarily governed by magnetic

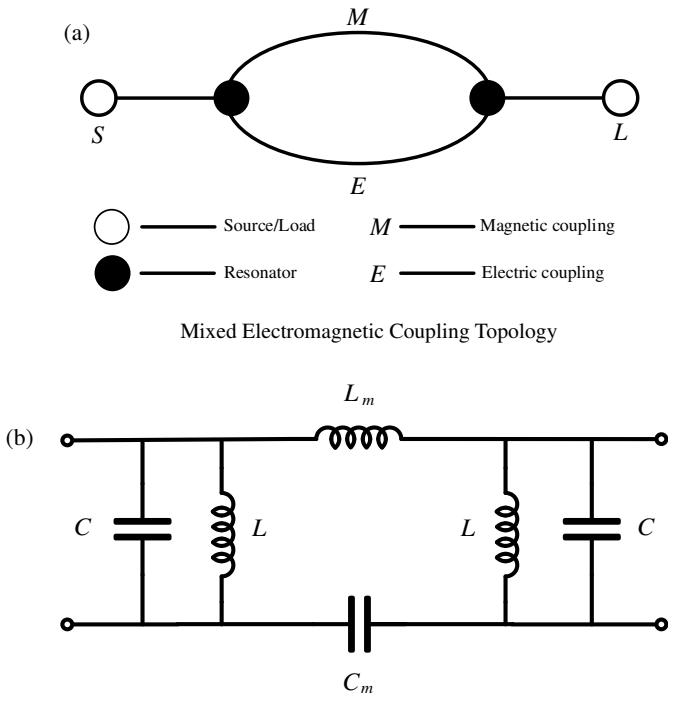

FIGURE 1. Second-order bandpass filter mixed coupling circuit.

interaction. The separation between these two frequencies reflects the strength of coupling between the resonators. Accordingly, the mixed coupling coefficient k_x can be defined as:

$$k_x = \frac{f_e^2 - f_m^2}{f_e^2 + f_m^2} = \frac{CL_m + LC_m}{LC + L_mC_m} \tag{3}$$

When the mutual capacitance and mutual inductance are much smaller than the self-capacitance and self-inductance, $C_m \ll C$ and $L_m \ll L$, the preceding expressions reduce to:

$$k_x \approx \frac{L_m}{L} + \frac{C_m}{C} = k_M + k_E \tag{4}$$

In this formulation, k_M denotes the magnetic coupling coefficient and k_E the electric coupling coefficient. This relationship illustrates that the mixed coupling coefficient essentially represents a linear superposition of electric and magnetic coupling. In practical structural design, when the mixed two coupling mechanisms share the same polarity, they reinforce each other, thereby enhancing the overall coupling strength and broadening the passband. Conversely, when their polarities are opposite, partial cancellation occurs, weakening the net coupling and potentially leading to complete cancellation in specific frequency ranges. Therefore, appropriately controlling the relationship between mutual inductance and mutual capacitance is critical in optimizing passband width and stopband suppression performance in filter design.

3. FILTER STRUCTURE DESIGN

The resonant unit employed in this work is a symmetrically folded structure derived from a conventional U-shaped hairpin

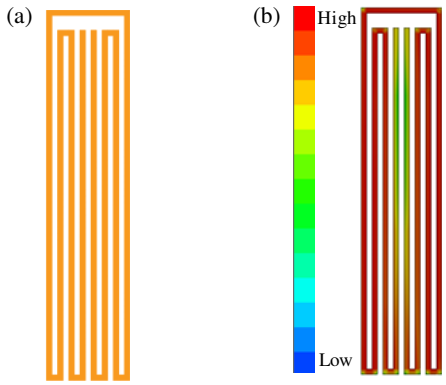

FIGURE 2. Resonator structure and current distribution. (a) Resonator structure. (b) Resonator current distribution.

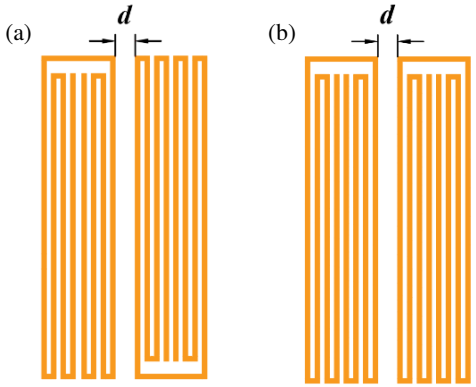

FIGURE 3. Resonator coupling structures. (a) Counter-directional coupling. (b) Co-directional coupling.

resonator. To address the issue of large physical size inherent in hairpin resonators, the resonant arms are further meandered and folded into an approximately closed-loop contour, separated by narrow gaps of approximately 0.15 mm, as depicted in Fig. 2(a). This folded configuration serves to increase the effective electrical length within a confined area, while the incorporation of multiple adjacent folded arms and narrow gaps along the loop causes the electric and magnetic field distributions in different structural regions to exhibit pronounced disparities. Fig. 2(b) shows the simulated current density distribution of the resonator at its operating frequency. The results indicate that the highest current concentration occurs along the curved arms on both sides, where strong magnetic field localization enhances magnetic coupling. In contrast, the central regions exhibit relatively weaker current density, with concentrated electric fields, establishing effective capacitive coupling paths. The overall symmetric, uniform current distribution confirms that the proposed structure exhibits well-balanced mixed electromagnetic coupling.

The relative orientation of adjacent resonators significantly influences the type and strength of coupling between them. As shown in Fig. 3, coupling configurations can be classified into two fundamental types based on the direction of current flow: co-directional coupling and counter-directional coupling. In the counter-directional coupling configuration, where the currents in the two resonators flow in opposite directions, the magnetic field circulations in the coupling region tend to cancel each other out, thereby reducing the magnetic induction effect. However, since the electric fields in the gap region maintain the same orientation, the fringing electric fields superimpose and reinforce each other, resulting in enhanced capacitive coupling. Consequently, the coupling in this configuration is primarily governed by electric-field interactions, with predominantly electric coupling. Conversely, in the co-directional coupling configuration, where adjacent resonators carry currents in the same direction, the magnetic fields in the coupling region are aligned and constructively superimpose, thereby strengthening the magnetic induction effect. Meanwhile, the electric fields become relatively opposed in direction, leading to partial cancellation of the fringing capacitance and a consequent reduction in electric coupling strength. As a result, magnetic interaction

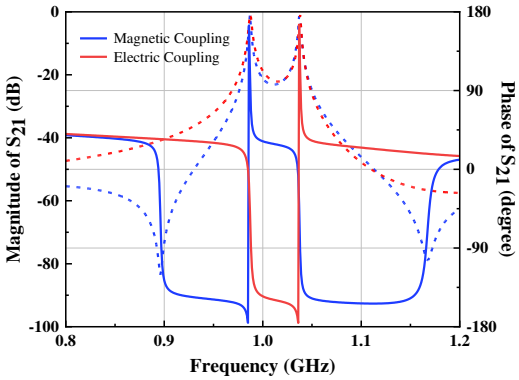

FIGURE 4. Amplitude and phase variation of electromagnetic field coupling.

becomes the dominant coupling mechanism in this configuration, demonstrating predominantly magnetic coupling behavior.

As the dominant nature of the coupling path switches, corresponding alterations occur in the frequency response. Specifically, the predominant effects of electric and magnetic coupling produce distinct frequency-domain characteristics. Fig. 4 presents the extracted magnitude and phase responses of S_{21} under electric-dominant and magnetic-dominant coupling states, obtained from two different resonator coupling configurations in the vicinity of the resonant frequency. It is observed that the magnitude characteristics of S_{21} remain largely consistent in both cases. However, near resonance, the phase undergoes an abrupt shift of approximately 180° in both configurations, yet in opposite directions. This contrasting phase behavior serves as a definitive indicator for distinguishing between the two coupling states, thereby providing crucial design guidance for the subsequent precise control of coupling polarity through optimized resonator layout. Following this analysis, further adjustment of the inter-resonator spacing significantly influences the coupling strength. In both co-directional and counter-directional coupling configurations, reduced separation between resonators enhances field interaction, leading to stronger coupling. Conversely, increased spacing weakens the electromagnetic fields in the coupling region, resulting in

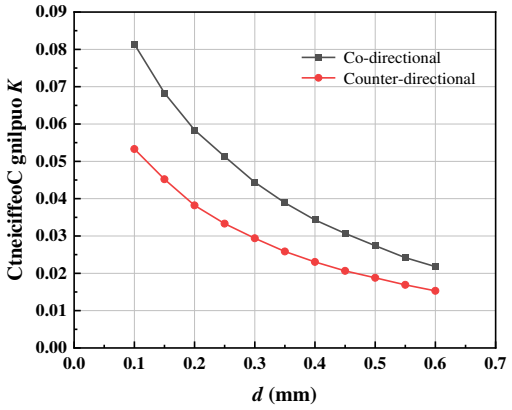

FIGURE 5. Variation of the coupling coefficient as a function of resonator spacing.

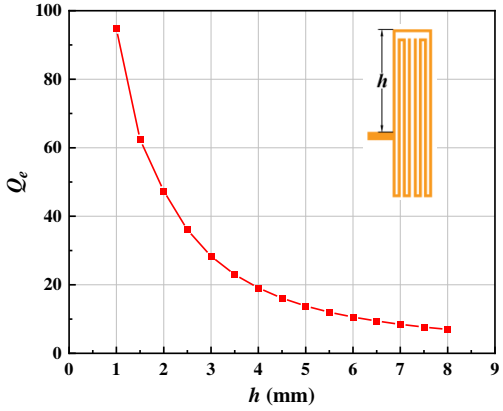

FIGURE 6. Variation of the external quality factor as a function of tap position.

diminished coupling strength. Fig. 5 illustrates the variation of the extracted coupling coefficient k as a function of resonator spacing for both coupling types. It is observed that the coupling coefficient increases substantially at smaller separations, demonstrating high sensitivity to structural spacing. This tunable characteristic provides a practical design approach for filter optimization, enabling precise control of coupling strength through strategic adjustment of resonator separation.

Furthermore, the tap position at the input port plays a critical role in determining the external quality factor (Q_e) and the filter's overall performance. The external quality factor can be extracted using a single-port structure, and it is calculated as [19]:

$$Q_e = \frac{\omega_0}{\Delta\omega_{\pm 90^\circ}} \tag{5}$$

where ω_0 represents the resonant angular frequency of the filter, and $\Delta\omega_{\pm 90^\circ}$ denotes the frequency bandwidth between the $\pm 90^\circ$ phase points relative to the resonant frequency. To further investigate the influence of tap position on the filter's transmission characteristics, this study examines variations in the extracted external quality factor with different tap positions (h), as shown in Fig. 6. Simulation results demonstrate that as h increases, the coupling strength between the port and resonator progressively enhances, resulting in a monotonic decrease in Q_e. Specifically, smaller h values correspond to weaker port coupling and higher Q_e, resulting in slower roll-off rates at the passband edges and limited out-of-band rejection. Conversely, appropriately increasing h reduces Q_e by enhancing coupling strength, accelerating the passband roll-off, and significantly improving out-of-band rejection performance. By considering bandwidth requirements, insertion loss control, and stopband suppression levels, optimized tap positioning can effectively enhance the spectral control capability and in-band transmission characteristics of the filter.

Based on a 14-pole Chebyshev filter synthesis approach, this paper presents an HTS microstrip filter with an operating band from 0.96 GHz to 1.06 GHz and a center frequency of 1.01 GHz. The theoretically calculated coupling coefficients between resonators are summarized in Table 1, where $M_{i,j}$ denotes the coupling coefficient between resonators i and j, and Q_e represents the external quality factor. A symmetric configuration is adopted in the design, ensuring that coupling coefficients between resonators at symmetric positions are identical, thereby simplifying the structure of the coupling matrix. This symmetrical approach eliminates the need for individual optimization of each coupling pair, significantly reducing the design complexity and improving overall efficiency. Based on the theoretical parameters, the filter structure is modeled and optimized using IE3D full-wave electromagnetic simulation. By adjusting the resonator length, inter-resonator spacing, and tap position, the structural layout is finalized to achieve optimized in-band insertion loss and out-of-band rejection performance. The filter is implemented on a double-sided HTS substrate with a dielectric constant of 9.8 and a thickness of 0.5 mm. Considering fabrication constraints, both the microstrip line width and gap width are designed to be greater than 0.1 mm to ensure structural reliability and manufacturing precision.

TABLE 1. Coupling coefficient of the 14th-order filter.

$M_{1,2} = M_{13,14}$	$M_{2,3} = M_{12,13}$	$M_{3,4} = M_{11,12}$	$M_{4,5} = M_{10,11}$
0.0795	0.0571	0.0531	0.0517
$M_{5,6} = M_{9,10}$	$M_{6,7} = M_{8,9}$	$M_{7,8}$	Q_e
0.0511	0.0503	0.0574	10.4

The overall filter structure, shown in Fig. 7, consists of 14 folded microstrip resonators cascaded linearly along the direction of propagation, resulting in a highly compact layout. Each resonator employs a folded geometry to form a closed current loop, achieving desirable resonant characteristics and high integration density within a confined area. Adjacent resonators are electromagnetically coupled through gaps, which are designed with non-uniform spacing to allow flexible control of inter-resonator coupling strength, thereby balancing wideband performance and out-of-band rejection. The entire structure maintains central symmetry, which helps optimize the electromagnetic field distribution, suppress spurious modes, and enhance frequency selectivity. In terms of coupling arrangement, co-directional coupling is utilized in the central region to

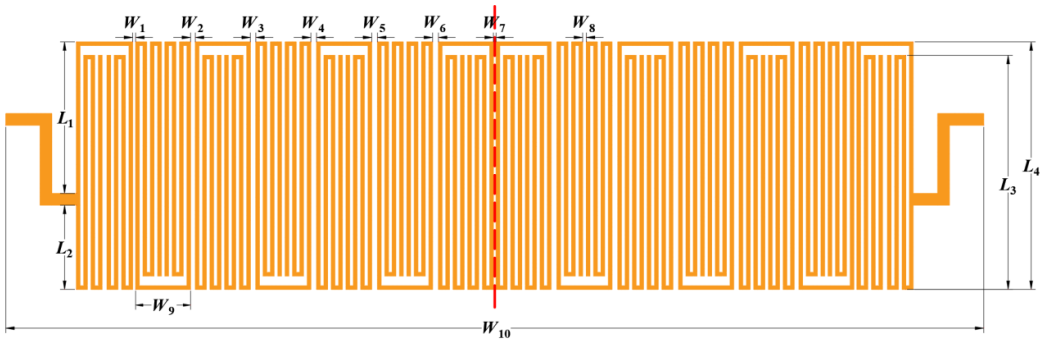

FIGURE 7. Schematic of the 14-pole symmetrical filter. ($W_1 = 0.12$, $W_2 = 0.19$, $W_3 = 0.22$, $W_4 = 0.23$, $W_5 = 0.23$, $W_6 = 0.23$, $W_7 = 0.11$, $W_8 = 0.15$, $W_9 = 2.25$, $W_{10} = 39.91$, $L_1 = 6.18$, $L_2 = 3.43$, $L_3 = 9.55$, $L_4 = 10.09$, unit: mm.)

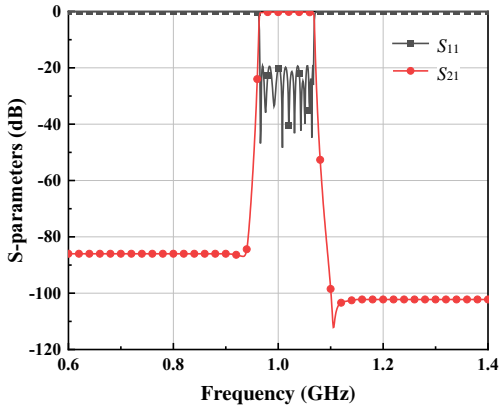

FIGURE 8. Filter simulation results.

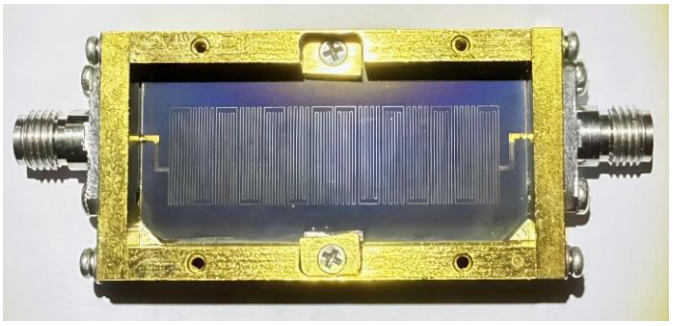

FIGURE 9. Photograph of the fabricated filter.

strengthen magnetic coupling, while counter-directional coupling is introduced at the edges to enhance electric coupling, collectively forming a cross-coupling configuration that further improves passband response and stopband suppression. Detailed dimensional parameters of the filter are provided in Table 1.

Figure 8 depicts the simulated S-parameters of the proposed filter. The results demonstrate that the filter, with a center frequency (f_0) of 1.01 GHz and a fractional bandwidth (FBW) of 9.9%, exhibits a flat passband from 0.96 to 1.06 GHz. Within this passband, the insertion loss (IL) is better than 0.2 dB and the return loss (RL) is greater than 19 dB. A sharp roll-off is observed at the band edges, accompanied by an out-of-band rejection exceeding 80 dB and a passband edge roll-off rate exceeding 60 dB/MHz. These characteristics confirm the superior performance of the proposed design.

4. FABRICATION AND MEASUREMENT OF FILTER

To validate the performance of the designed filter structure, a physical prototype was fabricated using high-precision planar lithography and subsequently measured. The fabrication process began with the creation of a photomask defining the filter circuit pattern via UV lithography, ensuring high pattern fidelity and uniform line widths. This mask pattern was then transferred onto a double-sided ceramic substrate coated with $YBa_2Cu_3O_7$ (YBCO) HTS thin film. The substrate, with a dielectric constant of 9.8, offers excellent high-frequency dielectric properties and thermal stability. The circuit pattern was etched on one side of the substrate to form the microstrip structures, while the opposite side served as a continuous ground plane. This ground plane was bonded to a metal shielding cavity using conductive adhesive to ensure adequate grounding. This grounding scheme enhances electromagnetic shielding, reduces spurious radiation interference, and contributes to more accurate and stable frequency responses during measurement. The final dimensions of the proposed filter were optimized to 39.91 mm × 10.09 mm, as shown in Fig. 9.

The measurement was performed using an HTS test platform. The filter was securely mounted onto a copper plate inside a cryogenic Dewar to maintain stability. Insulated coaxial cables were connected to the filter's input and output ports to establish reliable electrical interfaces. A closed-cycle cryocooler was then activated to cool the filter down to its superconducting transition temperature of 77 K, a critical step for achieving the optimal performance of the HTS material. Finally, the S-parameters were characterized using a vector network analyzer. The measured results, shown in Fig. 10, exhibit a well-defined passband spanning 0.96–1.06 GHz. The prototype exhibits an insertion loss of less than 0.4 dB, a return loss greater than 18 dB within the passband, and out-of-band rejection exceeding 78 dB. The close agreement between the measured and simulated results confirms the accuracy of the design methodology. The observed discrepancies between measured and simulated results are primarily attributed to fabrication tolerances in substrate thickness and microstrip line dimensions. These physical deviations consequently introduce errors in the filter's

TABLE 2. Comparison with published bandpass filters.

Ref.	f (GHz)	FBW (%)	IL (dB)	RL (dB)	Size ($\lambda_g \times \lambda_g$)	Order	Process technology	OBS (dB)
[1]	1.41	9.3	1.42	20	$0.160 * 0.210$	2	PCB	50
[7]	4.54	55.5	1.6	12.4	$0.370 * 0.590$	10	PCB	72
[21]	2.4	12.1	1.2	15	$0.247 * 0.145$	4	PCB	50
[22]	3.5	8.71	0.91	18	$0.280 * 0.700$	2	PCB	35
[23]	1.65	5	1.7	16	$0.110 * 0.220$	4	PCB	49
[24]	0.12	8.37	0.28	16.3	$0.063 * 0.062$	12	HTS	60
[25]	2.51	2.14	0.1	18	$0.670 * 0.490$	8	HTS	60
This work	1.01	9.9	0.4	18	$0.421 * 0.106$	14	HTS	78

λ_g: the guided wavelength at the center frequency f_0. OBS: Out-of-band Suppression.

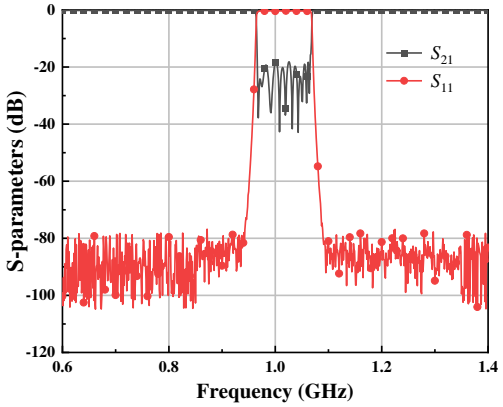

FIGURE 10. Measured results of the filter.

frequency response. Table 2 compares the key performance metrics of the proposed filter with those reported in recent literature. The results demonstrate that our design maintains favorable filtering characteristics while achieving low insertion loss, compact circuit size, high return loss suppression, and excellent out-of-band rejection. In contrast, other filters often struggle to balance bandwidth, loss, and overall dimensions, with many exhibiting either excessive size or higher insertion loss. Consequently, the proposed filter configuration demonstrates significant potential for practical applications, offering well-balanced overall performance.

5. CONCLUSION

This paper presents the design of a 14-pole compact HTS microstrip bandpass filter based on a mixed electromagnetic coupling mechanism. By employing a symmetrically folded resonator configuration combined with non-uniform coupling gaps and optimized coupling polarity, the proposed structure enables precise control over the electromagnetic coupling paths within a constrained footprint. This approach enhances the filter's coupling efficiency and improves the uniformity of the overall electromagnetic field distribution. The filter was fabricated using a double-sided YBCO HTS thin-film process, which provides excellent structural stability and miniaturization. Both simulated and measured results confirm that the filter operates within the 0.96–1.06 GHz band, with an insertion loss of less than 0.4 dB, an out-of-band rejection greater than 78 dB, and a steep passband roll-off rate exceeding 60 dB/MHz, demonstrating excellent overall performance. These findings validate the feasibility of the proposed design for high-performance, compact HTS microstrip filters, highlighting its strong potential for practical applications in modern communication systems and highly integrated microwave circuits.

REFERENCES

[1] Li, D., J.-A. Wang, Z. Chen, Y. Zhang, M.-C. Tang, and L. Yang, "Compact microstrip bandpass filter with sharp roll-off and broad stopband using modified 0° feed structure," *AEU — International Journal of Electronics and Communications*, Vol. 109, 17–22, 2019.

[2] Kadhom, M. J., "High selectivity tri-coupled line bandpass filter based on even- and odd-mode impedance modeling," *Progress In Electromagnetics Research C*, Vol. 161, 12–26, 2025.

[3] Guo, Y., L.-L. Qiu, L. Deng, Y. Wu, Y. Wang, and S. Huang, "Signal-interference-based quasi-reflectionless bandpass filter for wideband and high-selectivity," *International Journal of Circuit Theory and Applications*, Vol. 52, No. 7, 3144–3153, 2024.

[4] Kuo, J.-T., C.-L. Hsu, and E. Shih, "Compact planar quasi-elliptic function filter with inline stepped-impedance resonators," *IEEE Transactions on Microwave Theory and Techniques*, Vol. 55, No. 8, 1747–1755, 2007.

[5] Wang, J., S. Yu, X. Yang, and X. Liu, "Bandpass filter for 5G sub-6 GHz bands," *Progress In Electromagnetics Research Letters*, Vol. 116, 79–85, 2024.

[6] Ouyang, X. and Q.-X. Chu, "A mixed cross-coupling microstrip filter with multiple transmission zeros," *Journal of Electromagnetic Waves and Applications*, Vol. 25, No. 11-12, 1515–1524, 2011.

[7] Jiao, Y., H. Liu, H. Tian, R. Wang, and F. Yang, "Design of high order wideband bandpass filter with wide stopband based on hairpin ring resonator," *AEU — International Journal of Electronics and Communications*, Vol. 193, 155728, 2025.

[8] Wei, X.-B., Y. Shi, P. Wang, J.-X. Liao, Z.-Q. Xu, and B. C. Yang, "Miniaturized mixed-cross coupling bandpass filter with source-load coupling," *Journal of Electromagnetic Waves and Applications*, Vol. 26, No. 13, 1694–1699, 2012.

[9] Xiao, J.-K., M. Zhu, Y. Li, L. Tian, and J.-G. Ma, "High selective microstrip bandpass filter and diplexer with mixed electromagnetic coupling," *IEEE Microwave and Wireless Components Letters*, Vol. 25, No. 12, 781–783, 2015.

[10] Nwajana, A. O. and E. R. Obi, "Application of compact folded-arms square open-loop resonator to bandpass filter design," *Micromachines*, Vol. 14, No. 2, 320, 2023.

[11] Zhao, G., C. Li, M. Li, P. Zhang, Y. Yan, X. Mo, and Z. Tu, "A novel miniaturized image rejection bandpass filter basing on stepped-impedance resonators," *Progress In Electromagnetics Research Letters*, Vol. 112, 27–34, 2023.

[12] Ono, S., Y. Harada, T. Kato, A. Saito, J. H. Lee, H. Kinouchi, T. Oba, M. Yoshizawa, and S. Ohshima, "Fabrication and measurement of 5 GHz miniaturized 10-pole bandpass filter using superconducting microstrip quasi-spiral resonators," *Physica C: Superconductivity*, Vol. 468, No. 15-20, 1969–1972, 2008.

[13] Aghabagheri, S., M. Rasti, M. R. Mohammadizadeh, P. Kameli, H. Salamati, K. Mohammadpour-Aghdam, and R. Faraji-Dana, "High temperature superconducting YBCO microwave filters," *Physica C: Superconductivity and its Applications*, Vol. 549, 22–26, 2018.

[14] Ren, B., X. Liu, X. Guan, and Z. Ma, "High-selectivity high-temperature superconducting triband balanced bandpass filter using symmetric stub-loaded resonator," *IEEE Transactions on Applied Superconductivity*, Vol. 33, No. 8, 1–5, 2023.

[15] Ren, B., X. Guan, H. Liu, Z. Ma, and M. Ohira, "Highly selective and controllable superconducting dual-band differential filter with attractive common-mode rejection," *IEEE Transactions on Circuits and Systems II: Express Briefs*, Vol. 69, No. 3, 939–943, Mar. 2022.

[16] Huang, H., Y. Wu, J. Wang, Y. Bian, X. Wang, G. Li, X. Zhang, C. Li, L. Sun, and Y. He, "A wideband uhf high-temperature superconducting filter system with a fractional bandwidth over 108%," *Physica C: Superconductivity and Its Applications*, Vol. 550, 78–81, 2018.

[17] Zhang, T., J. Du, Y. J. Guo, and X. Sun, "A compact HTS bandpass microstrip filter with novel coupling structure for on-chip integration," *Physica C: Superconductivity*, Vol. 495, 69–73, 2013.

[18] Wu, D., B. Wei, B. Li, X.-B. Guo, X.-X. Lu, and B.-S. Cao, "Compact wide stopband superconducting bandpass filter using modified spiral resonators with interdigital structure," *Chinese Physics B*, Vol. 27, No. 6, 068502, 2018.

[19] Liu, H., B. Ren, S. Hu, X. Guan, P. Wen, and J. Tang, "High-order dual-band superconducting bandpass filter with controllable bandwidths and multitransmission zeros," *IEEE Transactions on Microwave Theory and Techniques*, Vol. 65, No. 10, 3813–3823, Oct. 2017.

[20] Hong, J.-S. and M. J. Lancaster, "Couplings of microstrip square open-loop resonators for cross-coupled planar microwave filters," *IEEE Transactions on Microwave Theory and Techniques*, Vol. 44, No. 11, 2099–2109, 1996.

[21] Afzali, B., H. Abbasi, F. Shama, and R. Dehdasht-Heydari, "A microstrip bandpass filter with deep rejection and low insertion loss for application at 2.4 GHz useful wireless frequency," *AEU — International Journal of Electronics and Communications*, Vol. 138, 153811, 2021.

[22] Chaudhary, G. and Y. Jeong, "Arbitrary prescribed flat wideband group delay absorptive microstrip bandpass filters," *IEEE Transactions on Microwave Theory and Techniques*, Vol. 69, No. 2, 1404–1414, 2021.

[23] Zakharov, A., S. Rozenko, L. Pinchuk, and S. Litvintsev, "Microstrip quazi-elliptic bandpass filter with two pairs of antiparallel mixed-coupled SIRs," *IEEE Microwave and Wireless Components Letters*, Vol. 31, No. 5, 433–436, 2021.

[24] Yu, X., W. Xi, S. Wu, and P. Yan, "A 12-pole VHF band high selective high temperature superconducting filter," *Superconductor Science and Technology*, Vol. 34, No. 1, 015002, 2020.

[25] Tan, C., Y. Wang, Z. Yan, X. Nie, Y. He, and W. Chen, "Superconducting filter based on split-ring resonator structures," *IEEE Transactions on Applied Superconductivity*, Vol. 29, No. 4, 1–4, 2019.